J Membrane Biol (2014) 247:897–908
DOI 10.1007/s00232-014-9725-1

Thermal Fluctuations in Amphipol A8-35 Particles: A Neutron Scattering and Molecular Dynamics Study

Moeava Tehei · Jason D. Perlmutter · Fabrice Giusti · Jonathan N. Sachs · Giuseppe Zaccai · Jean-Luc Popot

Received: 19 March 2014 / Accepted: 26 August 2014 / Published online: 10 September 2014

Abstract Amphipols are a class of polymeric surfactants that can stabilize membrane proteins in aqueous solutions as compared to detergents. A8-35, the best-characterized amphipol to date, is composed of a polyacrylate backbone with ~35 % of the carboxylates free, ~25 % grafted with octyl side-chains, and ~40 % with isopropyl ones. In aqueous solutions, A8-35 self-organizes into globular particles with a molecular mass of ~40 kDa. The thermal dynamics of A8-35 particles was measured by neutron scattering in the 10-picosecond, 18-picosecond, and 1-nanosecond time-scales on natural abundance and deuterium-labeled molecules, which permitted to separate backbone and side-chain motions. A parallel analysis was performed on molecular dynamics trajectories (Perlmutter et al., Langmuir 27:10523–10537, 2011). Experimental results and simulations converge, from their respective time-scales, to show that A8-35 particles feature a more fluid hydrophobic core, predominantly containing the octyl chains, and a more rigid solvent-exposed surface, made up predominantly of the hydrophilic polymer backbone. The fluidity of the core is comparable to that of the lipid environment around proteins in the center of biological membranes, as also measured by neutron scattering. The biological activity of proteins depends sensitively on molecular dynamics, which itself is strongly dependent on the immediate macromolecular environment. In this context, the characterization of A8-35 particle dynamics constitutes a step toward understanding the effect of amphipols on membrane protein stability and function.

Keywords Membrane proteins · Surfactants · Polymers · Molecular dynamics · QENS

Abbreviations

A8-35	An anionic amphipol of average molecular mass ~4.3 kDa, containing ~35 % free carboxylates, ~25 % octyl side-chains, and ~40 % isopropyl ones
APol	Amphipol
CAC	Critical association concentration
DAPol	A8-35 with per-deuterated side-chains
EINS	Elastic incoherent neutron scattering
HAPol	Natural abundance A8-35
INS	Inelastic neutron scattering
MD	Molecular dynamics
$\langle M_n \rangle$	Number-averaged molecular mass

M. Tehei
Centre for Medical Radiation Physics and Centre for Medical and Molecular Bioscience, University of Wollongong, Wollongong, NSW 2522, Australia

J. D. Perlmutter
Department of Physics, Brandeis University, 415 South Street, Waltham, MA 02453, USA

F. Giusti · J.-L. Popot (✉)
UMR 7099, Centre National de la Recherche Scientifique/Université Paris-7, Institut de Biologie Physico-Chimique (FRC 550), 13 rue Pierre et Marie Curie, 75005 Paris, France
e-mail: jean-luc.popot@ibpc.fr

J. N. Sachs
Department of Biomedical Engineering, University of Minnesota, 312 Church Street SE, Minneapolis, MN 55455, USA

G. Zaccai (✉)
Institut de Biologie Structurale, CEA/CNRS/UJF UMR5075, 38027 Grenoble, France
e-mail: zaccai@ill.fr

G. Zaccai
Institut Laue Langevin, 38042 Grenoble, France

mQ water	Water purified on a A10 Advantage Millipore System
MSD	Mean square displacement
OmpA, OmpX	Respectively outer membrane proteins A and X from *Escherichia coli*
QENS	Quasi-elastic neutron scattering
R_S	Stokes radius
SANS	Small-angle neutron scattering
SEC	Size exclusion chromatography

Introduction

Handling integral membrane proteins (MPs) in aqueous solution without compromising their stability can be difficult because detergents, customarily used to solubilize MPs, tend to inactivate them (see e.g., Bowie 2001; Garavito and Ferguson-Miller 2001; Gohon and Popot 2003; Popot 2010; Rosenbusch 2001). Amphipols (APols) have been developed as milder alternatives to detergents (Popot et al. 2011; Tribet et al. 1996; Zoonens and Popot 2014). They are constituted of polymer chains carrying hydrophobic and hydrophilic groups. The former adsorb onto the hydrophobic transmembrane surface of the protein (Althoff et al. 2011; Etzkorn et al. 2014; Huynh et al. 2014; Liao et al. 2013, 2014; Planchard et al. 2014; Zoonens et al. 2005), while the latter form the interface with the aqueous solution (Perlmutter et al. 2014). All amphipathic polymers, however, are not APols, and careful chemical design is essential to achieve the required properties (Popot et al. 2011; Zoonens and Popot 2014). In water, APol macromolecules assemble into particles similar in their size and overall organization to the micelles formed by the much smaller detergent molecules (Gohon et al. 2004, 2006; Perlmutter et al. 2011), but they do so at lower concentration because of the many hydrophobic chains that each molecule carries and the less severe entropic penalty resulting from loss of translational freedom (Giusti et al. 2012). Even though individual APol molecules are highly polydisperse (Giusti et al. 2014), they assemble into well-defined particles. The present study is concerned with APol A8-35, whose chemical structure is shown in Fig. 1 (Tribet et al. 1996).

A8-35 is currently the best-characterized APol in both its self-association properties and its interactions with membrane proteins (reviewed in Popot et al. 2011; Zoonens and Popot 2014). Individual A8-35 molecules have an average molecular mass of ~4.3 kDa (Giusti et al. 2014). In aqueous solutions, A8-35 has been shown to form well-defined globular particles with a molecular mass of ~40 kDa and a Stokes radius $R_S \approx 3.15$ nm, containing an average of 9–10 molecules and ~80 octyl chains (Gohon et al. 2004, 2006). The critical association concentration (CAC) of A8-35 has been determined by surface tension and Förster resonance energy transfer measurements to be ~0.002 g L^{-1} (in 100 mM NaCl, 20 mM Tris/HCl, pH 8.0; Giusti et al., 2012), implying that, under most experimental circumstances, nearly all A8-35 molecules in a preparation are self-organized. Molecular dynamics (MD) simulations suggest that A8-35 particles adopt a micelle-like organization, with a hydrophobic core mainly constituted of octyl chains and a hydrophilic, carboxylate-rich surface with significantly stiffer dynamics on the nanosecond to microsecond time-scales than the surface of detergent micelles (Perlmutter et al. 2011).

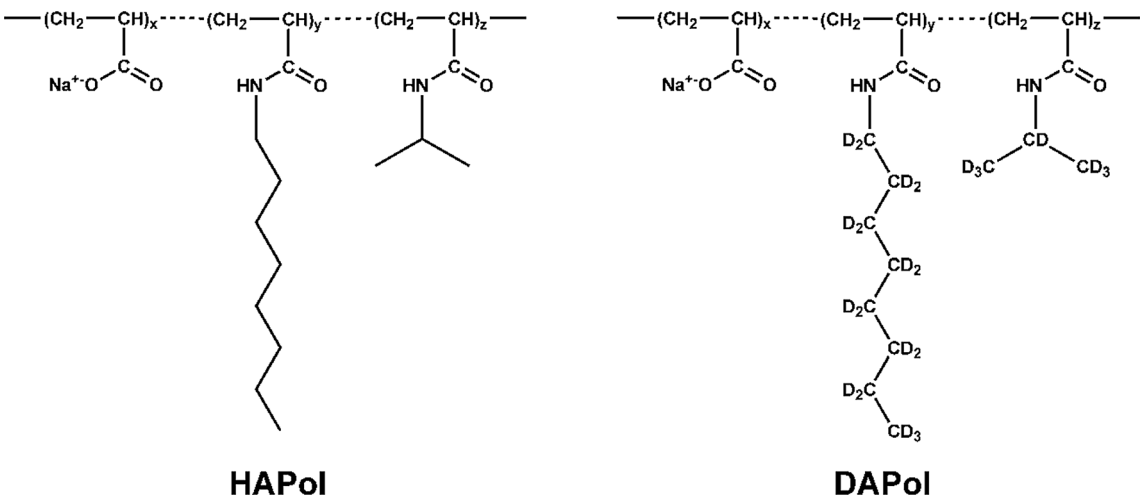

Fig. 1 Chemical structures of unlabeled (Tribet et al. 1996a) and partially deuterated A8-35 (Gohon et al. 2006). The various moieties are distributed randomly along the chain, in the proportion $x \approx 0.35$, $y \approx 0.25$, and $z \approx 0.40$. *Left panel* natural abundance A8-35 (HAPol). *Right panel* A8-35 with a natural abundance backbone and deuterated side-chains (DAPol)

As a rule, trapping with A8-35 preserves the functionality and ligand-binding properties of MPs (Popot et al. 2011; Tribet et al. 1996; Zoonens and Popot 2014). However, it has been observed that the enzymatic cycle of the sarcoplasmic calcium pump from twitch muscle (Ca^{2+}-ATPase; SERCA1a) is reversibly inhibited following transfer to various APols, while the protein is strongly stabilized against denaturation (Champeil et al. 2000; Picard et al. 2006). Various observations have led to the proposal that the two effects are linked, both resulting from the free energy cost of reorganizing the polymer's backbone during large-scale transconformations of the protein's transmembrane domain, a phenomenon dubbed the "Gulliver effect" (for discussions, see Perlmutter et al. 2014; Popot et al. 2011; Zoonens and Popot 2014). The biological activity of proteins depends sensitively on their molecular dynamics, which is itself strongly dependent on their immediate environment (Tehei et al. 2005; Tehei and Zaccai 2005; Zaccai 2013). In view of optimizing the design and use of APols, it is of interest to understand the respective effects of the polymer's backbone and side-chain dynamics on that of the protein, as well as the effect of binding to the protein on the polymer's dynamics. The experimental characterization of A8-35 particle dynamics reported here constitutes one step toward investigating these issues, which are also being addressed in parallel by MD calculations (Perlmutter et al. 2011, 2014, and present work).

Neutron scattering measurements provide experimental dynamics data on a picosecond to nanosecond time-scale and an ångstrøm length-scale. Because the scattering cross section of hydrogen is much larger than that of deuterium; motions of different parts of a polymer can be discriminated by selective isotope labeling. In the present work, we have measured the thermal dynamics of A8-35 particles made up of unlabeled molecules (HAPol; Fig. 1, left) or of molecules in which the hydrogen atoms in the octyl and isopropyl side-chains are replaced by deuterium (DAPol; Fig. 1, right; Gohon et al. 2004, 2006). The HAPol sample yielded information on all backbone and side-chain group motions, whereas the DAPol sample data were dominated by the backbone. Experimental results and MD simulations data converge, from their respective time-scales, in describing the A8-35 particles as having a more fluid hydrophobic core predominantly containing the octyl chains, surrounded by a more rigid shell made up predominantly of the hydrophilic polymer backbone. The core fluidity was found to be comparable to that of the natural lipid environment around the MP bacteriorhodopsin (BR), measured previously by neutron scattering (Frölich et al. 2009). The data presented here provide an important control for future neutron scattering studies of the dynamics of APol-trapped MPs, as well as baseline values for characterizing the effects of binding to MPs on APol dynamics.

Materials and Methods

Amphipols

Amphipol A8-35 (sodium salt) was synthesized as described (Gohon et al. 2004, 2006), either in unlabeled form (HAPol) or in a form whose polyacrylate backbone is unlabeled, and the octylamine and isopropylamine chains are deuterated (DAPol). The proportions of the three types of units (*cf.* Fig. 1) in the two batches used for the present experiments were the following: x (percentage of free carboxylate), $\sim$35 %; y (octyl chains), $\sim$25 %; and z (isopropyl): $\sim$40 %. In aqueous solutions at pH $\geq$ 7, the carboxylates are totally ionized (Gohon et al. 2004). The solution properties of HAPol and DAPol, as analyzed by size exclusion chromatography, dynamic light scattering, and analytical ultracentrifugation, as well as their small-angle elastic neutron scattering profiles and contrast-matching points have been described by Gohon et al. (2004, 2006). Determination of the CAC of A8-35 is described by Giusti et al. (2012). ^{1}H,^{1}H and ^{1}H,^{13}C NMR spectra of HAPol and DAPol are shown in Giusti et al. (2014).

Sample Preparation for Neutron Scattering

HAPol and DAPol were dialyzed against 100 % D_2O and freeze-dried. Before use, the lyophilized powders were dissolved at 240 g L^{-1} overnight at 4 °C, under stirring, in 20 mM Tris/HCl, 100 mM NaCl D_2O solution, pD 8.0. The solutions were placed in aluminum sample containers matching the size of the neutron beam available on the instrument. To verify that no loss of material had occurred, samples were weighed before and after the neutron scattering experiments. No losses were detected for any of the samples.

Neutron Scattering Measurements

Experiments were carried out using two spectrometers at the Institut Laue-Langevin (ILL) (http://www.ill.eu/): (i) the time-of-flight spectrometer IN6, with energy resolutions of 90 and 50 μeV ΔE full width at half-maximum (FWHM), and (ii) the backscattering spectrometer IN16 (0.9 μeV ΔE FWHM) (Table 1). All experiments were performed at 280 K, a temperature that provides good signal-to-noise ratios for both EINS and QENS, and at which the samples are soluble and stable. The scattering was measured over a wave-vector range of 0.44 $Å^{-1} < Q < 1.80$ $Å^{-1}$, Q being the wave-vector transfer modulus. A vanadium sample (a purely elastic scatterer) was measured to define the instrument resolution and detector efficiency. Spectra were corrected for detector efficiency and sample container and buffer

Table 1 Characteristics of the spectrometers used in the present work

Spectrometer	Wavelength (Å)	Measured Q-range (Å^{-1})	Associated length-scale $1/Q$ (Å)	Energy resolution (μeV)	Associated time-scale up to
IN6	5.12	0.58–1.65	0.61–1.72	90	~10 ps
IN6	5.90	0.58–1.65	0.61–1.72	50	~18 ps
IN16	6.27	0.44–1.80	0.55–2.27	0.9	~1 ns

scattering, normalized, grouped, and converted to $S(Q,\omega)$ data using the LAMP data reduction routines (http://www.ill.eu/data_treat/lamp/the-lamp-book/). Sample transmissions were >90 %, so that multiple scattering could be neglected.

Data Analysis

An atomic mean square displacement (MSD) value $\langle u^2 \rangle$ describing averaged single particle motions was calculated from the Q-dependence of the elastic part of the dynamic structure factor, $S(Q,0 \pm \Delta E)$ by the Gaussian approximation:

$$S(Q, 0 \pm \Delta E) \approx \exp\left(-\frac{1}{6}\langle u^2 \rangle Q^2\right). \quad (1)$$

Depending on the geometry of the motion, the approximation is valid for any motion localized in the length–time window of the spectrometer, and it holds up to $\langle u^2 \rangle \cdot Q^2 \approx 2$. The MSD is then obtained from the slope of the logarithm of the scattered intensity:

$$\langle u^2 \rangle = -6\frac{\partial \ln S(Q, 0 \pm \Delta E)}{\partial Q^2}. \quad (2)$$

Note that in the above definition, $\langle u^2 \rangle$ is the time-dependent MSD in the long-time limit (in this case the resolution time of the instrument) for the particle trajectory (Zaccai 2011).

In the quasielastic region of the spectra, the calculated scattering function, $S_{\text{calc}}(Q,\omega)$, has been described by Bée (1988):

$$S_{\text{calc}}(Q, \omega) = DW.S_{\text{diff}}(Q, \omega), \quad (3)$$

where DW is a Debye–Waller factor that accounts for vibrational modes and $S_{\text{diff}}(Q,\omega)$ is a diffusive contribution. The DW factor is simply a scaling factor in ω-space that does not modify the shape of the quasielastic scattering function. $S_{\text{calc}}(Q,\omega)$ can be written as follows:

$$S_{\text{calc}}(Q, \omega) = DW\left[A_0(Q)\delta(\omega) + \sum_{i=1}^{n} A_i(Q)L(\Gamma_i, \omega)\right], \quad (4)$$

where $A_0(Q)$ and $L(\Gamma_i,\omega)$ are the elastic and diffusive contributions to the scattering function. The diffusive contributions can be described by Lorentzian functions:

$$L(\Gamma_i, \omega) = \frac{1}{\pi}\frac{\Gamma_i(Q)}{\Gamma_i(Q)^2 + \omega^2} \quad (5)$$

where Γ_i is the half-width at half-maximum (HWHM) of the Lorentzian peak. The measured scattering function, $S_{\text{meas}}(Q,\omega)$, is obtained by convoluting $S_{\text{calc}}(Q,\omega)$ with the energy resolution of the spectrometer, $S_{\text{res}}(Q,\omega)$, determined by the vanadium sample:

$$S_{\text{meas}}(Q, \omega) = e^{-\hbar\omega/(2k_B T)}[S_{\text{calc}}(Q, \omega) \otimes S_{\text{res}}(Q, \omega)] + B_0, \quad (6)$$

in which $e^{-\hbar\omega/(2k_B T)}$ is a detailed balance factor and B_0 an inelastic background caused by vibrational modes of lowest energy, also called phonons in crystals (Bée 1988).

Molecular Dynamics Simulations

A complete description of the methods used in the molecular dynamics simulations is available in Perlmutter et al. (2011). Briefly, the simulations were done using a two-step strategy. First, a coarse-grained simulation was performed using the Martini coarse-grained force field (Marrink et al. 2007) and parameters developed in Perlmutter et al. (2011). Using the coarse-grained model, 4 μs of simulation could be performed, during which APol particles formed de novo from separate polymer strands. In the second step, the coordinates of the coarse-grained model were used as the initial configuration for a more detailed all-atom simulation using the CHARMM force field (MacKerell et al. 1998). During this "reverse coarse-graining", all-atom water molecules and sodium counter ions were added. The all-atom simulations were run for 45 ns. The analysis presented here is for the second step of the simulation. Among the three types of sequences considered in Perlmutter et al. (2011), the 'random grafting' one was used for the present analysis.

Results

Experiments were performed to examine a range of length- and time-scales, defined by the properties of the spectrometers used (Table 1). All experiments were performed in D_2O in order to minimize the incoherent scattering

contribution of the solvent. Because of different H-bonding energies compared to H_2O, D_2O can exert an isotopic effect on solution structures and interactions. In certain proteins, for example, it favors aggregation. The SANS contrast variation data on APols, however, establish that the particle size and shape in solution is identical in both solvents (Gohon et al. 2004, 2006). D_2O has a stabilizing effect on structures and has been shown to influence macromolecular dynamics in solution (Tehei et al. 2001). Using only neutron scattering, it is technically impossible to assess whether D_2O modifies APol dynamics with respect to H_2O, because the signal-to-noise ratio in H_2O would be too small for the measurements to be carried out. The goal of the present investigation, however, is to compare backbone and side-chain dynamics under identical conditions. Sample concentrations were ~ 240 g L^{-1}.

Subtraction of the D_2O buffer spectra from the spectra measured for the A8-35 solution yields a valuable approximation of the scattering signal from the A8-35 particles. In the HAPol sample, this signal corresponds to the average contributions of all A8-35 atoms, but primarily the ^1H, 30 % of which are in the backbone, 42 % in the octyl side-chains, and 28 % in the isopropyl ones. In the DAPol sample, where the side-chains are deuterated, the signal is dominated by the backbone hydrogen atoms; the side-chain/backbone incoherent signal ratio for DAPol was estimated to be <10 %.

Following the procedures outlined in "Materials and Methods" section, atomic mean square displacements (MSDs) were extracted from the analysis of the Elastic Incoherent Neutron Scattering (EINS). Analysis of the Quasi-Elastic Neutron Scattering (QENS) yielded self-diffusion coefficients, relaxation times, and geometries for different motions.

The EINS from HAPol and DAPol, plotted as the logarithm of the intensity versus scattering vector squared for the two time-scales of IN6, is shown in Fig. 2. The MSD ($\langle u^2 \rangle$) values calculated from the slopes are given next to the plots.

For the HAPol sample at 50- and 90-μeV resolution, two Lorentzians could be fitted to the QENS for each scattering vector Q value. Their half-width, Γ (see "Materials and Methods" section), is plotted in Fig. 3 as a function of Q^2. QENS data for the DAPol sample were well fitted by a single Lorentzian at both resolution conditions.

For HAPol samples, at 90-μeV resolution, both Γ values are approximately flat with Q^2, indicating local reorientational motions (Fig. 3, left). The mean values of 0.60 and 0.05 meV correspond to correlation times of 1.1 and 13.2 ps, respectively. In contrast, the Lorentzians obtained at 50-μeV resolution (Fig. 3, right) revealed jump-diffusion motions (diffusion between sites, with a mean residence time τ_0 at each site):

$$\Gamma = \frac{DQ^2}{1 + DQ^2\tau_0}, \tag{7}$$

where D represents the internal diffusion coefficient. This equation yields $\tau_0 = 1.55 \pm 0.08$ ps and $D = 2.46 \pm 0.26 \times 10^{-4}$ cm^2 s^{-1} for Γ_1 (*blue squares*) and $\tau_0 = 17.47 \pm 0.44$ ps and $D = 2.69 \pm 0.29 \times 10^{-5}$ cm^2 s^{-1} for Γ_2 (*red circles*).

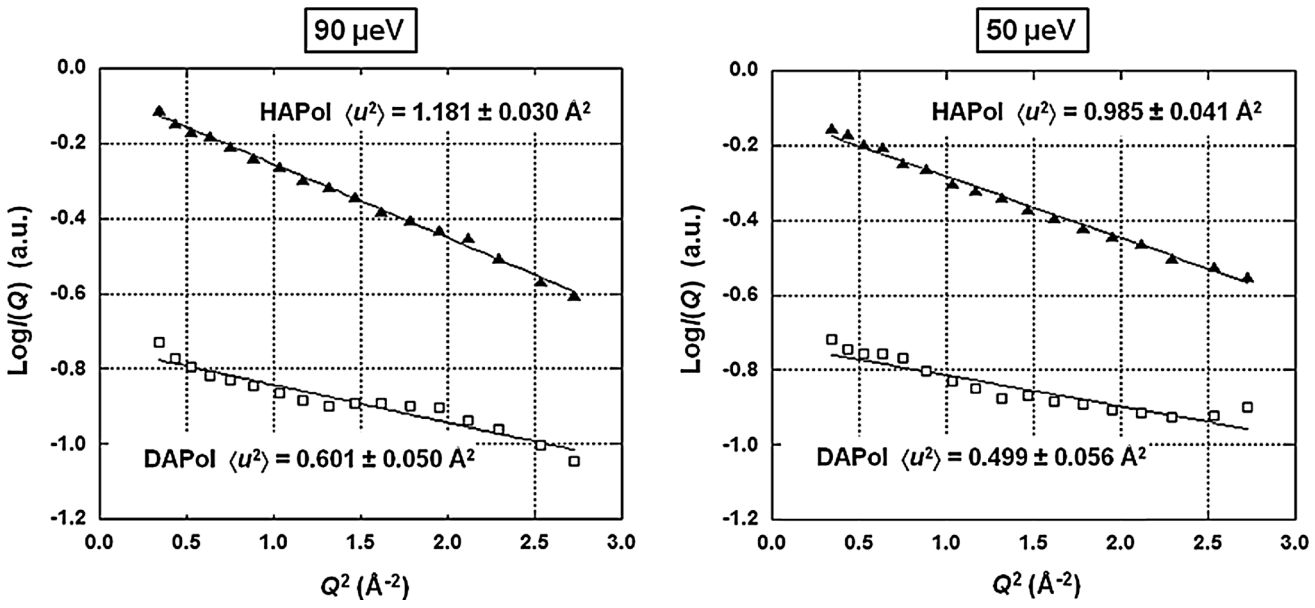

Fig. 2 EINS from HPol and DAPol. Logarithm of the normalized elastic intensity versus scattering vector squared measured on IN6 at 90 μeV (*left*) and 50 μeV (*right*), at 280 K, with corresponding linear fits. The range of the fits corresponds to $0.55 \leq \sqrt{Q^2 < u^2 >} \leq 1.73$

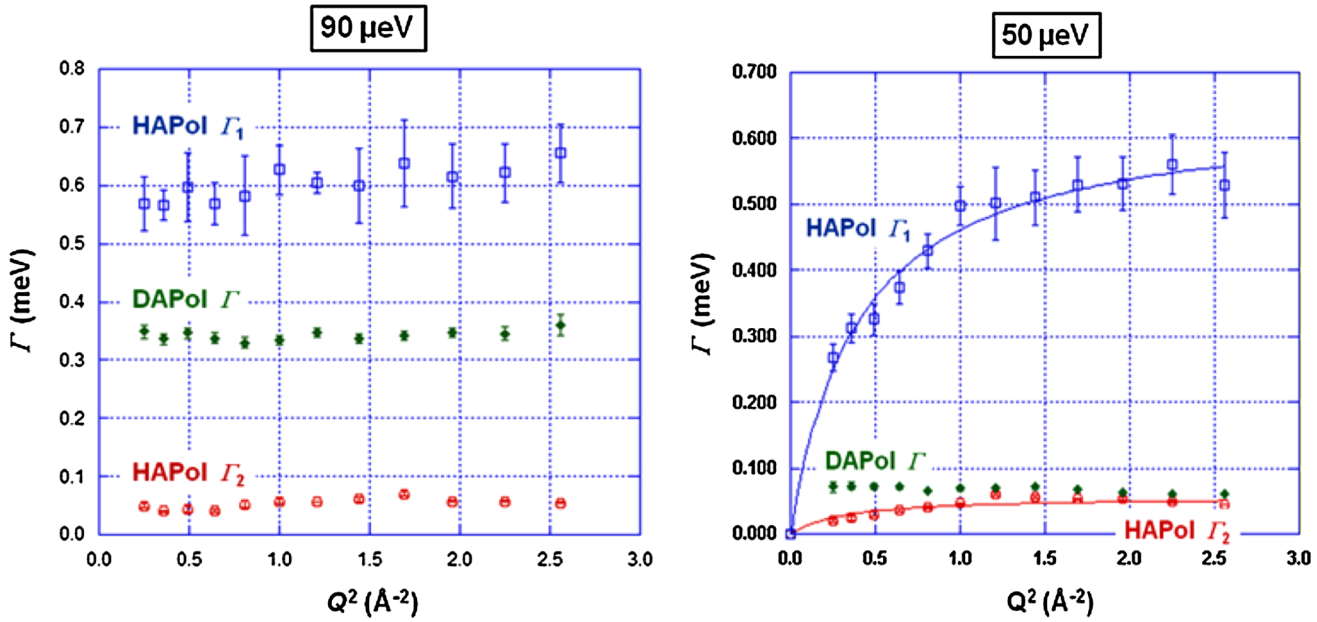

Fig. 3 Analysis of the QENS spectra from IN6 at 280 K. *Left panel* 90–μeV resolution; *right panel* 50–μeV resolution. HAPol sample. Half-widths at half-maximum, Γ_1 (*blue squares*) and Γ_2 (*red circles*), of the two Lorentzians fitted to the QENS spectrum plotted as a function of Q^2. The 'jump diffusion' model fit is shown for the 50-μeV resolution data (*right panel*). DAPol sample (*green diamonds*). Γ value for the one-Lorentzian fit to the QENS spectrum for the two resolution conditions (Color figure online)

For the DAPol samples, a flat dependence of Γ on Q^2 was found for both resolution conditions (Fig. 3). The mean values of 0.34 and 0.068 meV correspond to respective correlation times of 1.9 and 9.7 ps.

QENS on HAPol was also measured on IN16 (0.9-μeV resolution, ~1-ns time-scale). The QENS was well fitted by a single Lorentzian, whose half-width at half-maximum is plotted versus Q^2 in Fig. 4. The linear dependence of Γ on Q^2 indicates that on the time-scale of ~1 ns, macromolecular translation of the A8-35 particle as a whole dominates the QENS. A translational diffusion coefficient, $D_T = (4.45 \pm 0.11) \times 10^{-7}$ cm^2 s^{-1} was calculated from the plot. Since for self-diffusion the different parts of the A8-35 molecules move together, only the natural abundance sample (for which the signal-to-noise ratio is most favorable) was measured on IN16.

The molecular dynamics simulations allow one to investigate the dynamics of specific components of the A8-35 particle. Fig. 5 shows the autocorrelation of the carbon–hydrogen bond vectors, with the overall particle translation and rotation removed. These autocorrelation functions were fit to a double exponential:

$$f(\tau) = a\mathrm{e}^{-\tau/t_1} + (1-a)\mathrm{e}^{-\tau/t_2},$$

where τ is the lag time between frames and t_1 and t_2 are the characteristic times, listed in Table 3. This analysis clearly demonstrates that the dynamics of the backbone is predicted to be significantly slower than that of the side-chains.

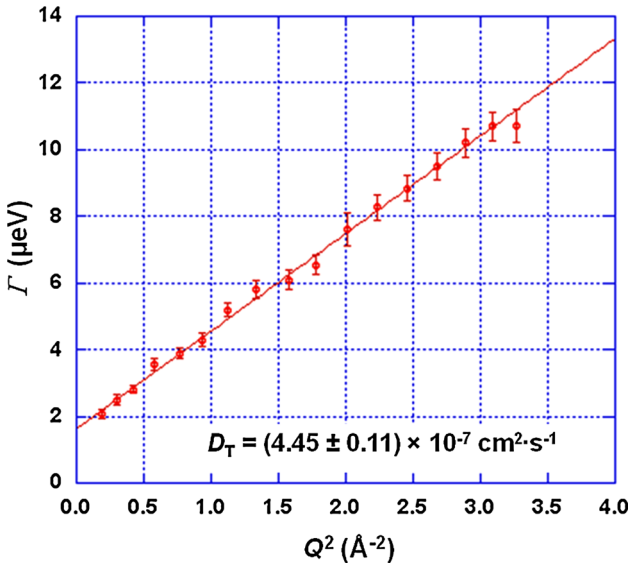

Fig. 4 Half-width at half-maximum, Γ, of the Lorentzian fitted to the QENS spectrum of HAPol measured on IN16 at 280 K, plotted as a function of Q^2

In Fig. 6 (bottom), the structure of the A8-35 particle is described by the time-averaged radial density of its components, plotted as a function of distance from the particle center, along with the distributions of water molecules and sodium counterions. As can also be observed in Fig. 6 (top), which shows a snapshot of an all-atom MD simulation, the octyl side-chains localize to the particle center, forming a

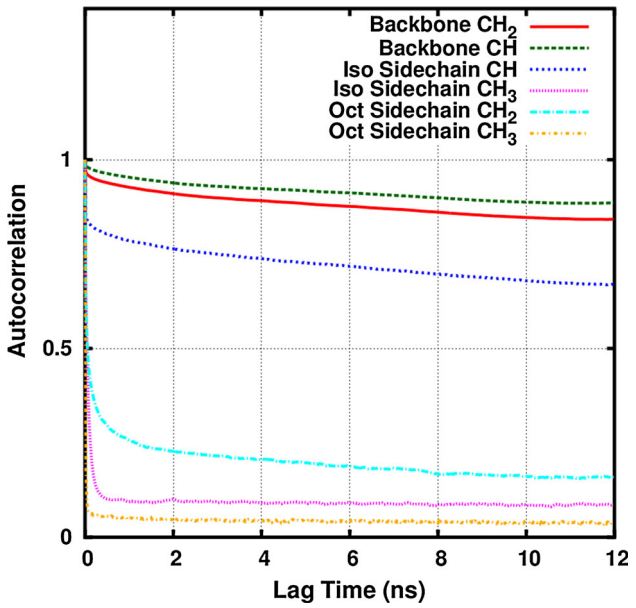

Fig. 5 Autocorrelation functions for different carbon–hydrogen bond vectors in the MD model of an A8-35 particle

hydrophobic core, whereas the isopropylamine side-chains and ungrafted carboxylates occupy the surface. The water density is near zero at the particle center and gradually rises to the bulk value outside the particle. The sodium counterions are clearly enriched at the particle periphery, relative to the particle core or bulk solution, and their distribution closely follows that of the free carboxylates.

Discussion

Incoherent neutron scattering by A8-35 is dominated by the motions of ^{1}H nuclei, which scatter much more intensely than any other nucleus, including deuterium in the isotope-labeled sample. In the time-scale examined, the thermal motions of H reflect the motions of the CH, CH_2, and CH_3 moieties with which they are associated. Samples were in D_2O and buffer scattering was subtracted, so that to a good approximation the HAPol data provided information on the motions of all groups in the polymer that carry nonexchangeable hydrogen atoms, and the DAPol data provided information on backbone group motions.

A8-35 Assembles into Well-Characterized Particles in the Neutron Scattering Conditions

The particles formed by A8-35 in aqueous buffers have been characterized by complementary biophysical methods, including analytical ultracentrifugation and small-angle neutron scattering (SANS) using contrast variation

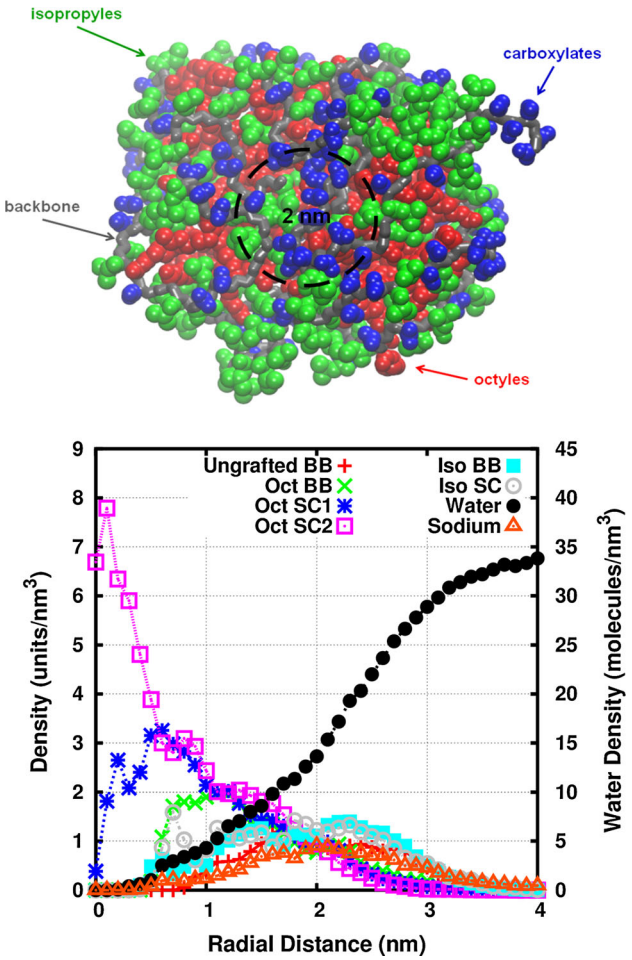

Fig. 6 *Top* snapshot image of an all-atom model of A8-35 particle formed by in silico self-assembly after 4 μs of coarse-grained MD calculation followed by reverse coarse-grained simulation (from Perlmutter et al. 2011). Water, counterions, and APol hydrogens have been omitted. The backbone is in *gray*, free carboxylates in *blue*, isopropyl grafts in *green*, and octyl grafts in *red*. The *dotted line* is a *circle* with radius 1 nm. *Bottom.* Radial distribution of the various moieties of A8-35 in the particle and of water molecules and Na^+ ions. Data extracted from all-atom MD trajectories for particles made up of A8-35 (random distribution of the various groups) after coarse-grained and reverse coarse-grained simulations (Perlmutter et al. 2011). The density for the A8-35 moieties is plotted for six distinct molecular groups, corresponding to backbone segments (BB), either ungrafted, grafted with isopropylamine (Iso BB), or grafted with octylamine (Oct BB), and to side-chain ones, there being one side-chain group per isopropyl graft (Iso SC) and two per octylamine graft (Oct SC1, Oct SC2), the latter corresponding, respectively, to the four methylenes closer to the backbone and to the three distal methylenes and the methyl group (see Perlmutter et al. 2011) (Color figure online)

(Gohon et al. 2004, 2006; reviewed in Popot et al. 2011; Zoonens and Popot, 2014). At pH $\geq$ 7, all carboxylates are ionized (Gohon et al. 2004). The highly soluble polymer self-assembles into particles of average molecular mass

Table 2 A comparison of the expected and measured diffusion coefficient of HAPol particles under QENS experimental conditions

Parameters	Value
Measured ratio of the viscosities in D_2O and H_2O solvents. $\eta_{ratio} = \eta_{D2O}/\eta_{H2O}$	1.212
Partial specific volume (Π')[a]	0.866 mL g^{-1}
Concentration $(C)^{(b)}$	240 g L^{-1}
Particle volume fraction. $\phi = \Pi' \times C$[b]	21 % v/v
Diffusion coefficient in H_2O at infinite dilution (D_0)[c]	6.80×10^{-7} cm^2 s^{-1}
Expected apparent diffusion in D_2O, calculated as $D_{Cal\text{-}App} = D_0/\eta_{ratio} \times 1.27 \times (1 - 2\phi)$	4.16×10^{-7} cm^2 s^{-1}
Measured diffusion coefficient in D_2O (QENS)[b]	$(4.45 \pm 0.11) \times 10^{-7}$ cm^2 s^{-1}

[a] Data from Gohon et al. (2004)
[b] From the present work
[c] From Gohon et al. (2006)

~40 kDa, each made up of 9–10 macromolecules and containing 75–80 octyl chains. Interestingly, the particles are much more monodisperse than the macromolecules from which they are formed. They have a radius of gyration of ~2.4 nm, and a Stokes radius of ~3.15 nm. SANS revealed that they are globular.

The experimental translational diffusion coefficient D_T obtained here on IN16 is $(4.45 \pm 0.11) \times 10^{-7}$ cm^2 s^{-1}. It has been shown previously that the calculated apparent self-diffusion coefficient, $D_{Cal-App}$, is given by

$$D_{Cal-App} = D_{0/}\eta_{ratio} \times 1.27 \times (1-2\phi),$$

where D_0 is the diffusion coefficient in H_2O at infinite dilution, η_{ratio} the ratio of the viscosities in D_2O and H_2O solvents, and ϕ is the particle volumic fraction (Perez et al. 1999; Venkatesan et al. 1985). Using the parameters in Table 2 (from data in Gohon et al. 2004, 2006) yields $D_{Cal-App} = 4.16 \times 10^{-7}$ cm^2 s^{-1}, which is in good agreement with the experimental value obtained in the present work. This is an important control, confirming that APol particles of similar properties to the ones characterized previously are still present at the high concentration required for the present measurements. It is quite remarkable that A8-35 particles remain essentially the same in the 1–10-g L^{-1} range (Gohon et al. 2006), at ~240 g L^{-1} (present work), and down to 0.002 g L^{-1} (Giusti et al. 2012), which is over six orders of magnitude of concentration. It indicates that they occupy a very large region of the phase diagram of A8-35, which is of great interest for experiments where MP/APol complexes must be highly concentrated, such as for the present kind of measurements, in crystallization attempts (Charvolin et al. 2014), and in solid-state NMR or some light spectroscopy experiments (see e.g. Polovinkin et al. 2014).

Mean Square Displacements and the Dynamic Structure of the A8-35 Particle

A picture of the A8-35 particle obtained after a 4-μs coarse-grained MD simulation followed by an all-atom MD simulation, consistent with biophysical data, is shown in Fig. 6 (top). It shows the octyl side-chains predominantly in the hydrophobic center of the particle and an outer hydrophilic shell comprising most of the underivatized carboxylates, in keeping with a quantitative analysis of the radial distribution of these various moieties, of water molecules, and of sodium ions in all-atom MD simulations (Fig. 6, bottom).

The MSDs calculated from the EINS data include vibrational as well as conformational sampling motions in the 10- and 18-ps time-scales (Fig. 2). At 280 K (~7 °C), the MSD measured for DAPol (~0.5 $Å^2$) is half that of HAPol (~1 $Å^2$) (Fig. 2), indicating that the side-chains contribute significantly larger conformational fluctuations than the backbone groups. HAPol values are very close to those for lipid MSDs measured recently by QENS, at 280 K and high hydration, on IN6 at 50-μeV resolution (Natali, private communication). At ~1 $Å^2$, they are significantly larger than values for proteins, for example, under similar conditions. The MSD measured for HAPol (Fig. 2) can be extrapolated to longer time-scales from data on other systems by assuming that similar motion classes are sampled. Lipid bilayer MSD increases by a factor of ~2 between the 18-ps and 0.1-ns time-scales (Natali et al. 2005, and F. Natali, private communication). In a neutron study of a polysaccharide over three different time-scales, the MSD increased by a factor of ~2 between the ps and ns time-scales (Jasnin et al. 2010). These data lead one to expect, for HAPol, MSD values for longer sampling times of ~2 $Å^2$, suggesting similar MSDs for lipids and the core of the A8-35 particle when adjusted to the ns time-scale.

Bond autocorrelation functions for different A8-35 moieties extracted from the all-atom MD trajectories of Perlmutter et al. (2011) are shown in Fig. 5. The functions could be fitted well with double exponentials, whose respective characteristic times are given in Table 3. Taken together, the QENS and MD data indicate that, on the vibrational as well as the longer time-scale of conformational fluctuations, the A8-35 particle can be described in terms of a softer hydrophobic core surrounded by a more

Table 3 Characteristic times for the double-exponential fits of the autocorrelation data in Fig. 5

Bond vector	t_1 (ns)	t_2 (ns)
Backbone C–H	0.28	114
Backbone C_α-H	0.53	156
Isopropyl side-chain methine	0.03	64
Isopropyl side-chain methyl	0.06	67
Octylamine side-chain methylene	0.06	19
Octylamine side-chain methyl	0.01	33

rigid hydrophilic outer shell that forms the interface with water. MD data suggests that the surface of A8-35 particles is more viscous than that of detergent micelles and even that of lipid bilayers (Perlmutter et al. 2011).

The QENS analysis provides more information on the types of thermal motion that the CH, CH_2, and CH_3 groups are undergoing in A8-35 particles (Figs. 3, 4), while confirming the higher mobility of the side-chains when compared to the polymer backbone. Jump-diffusion motions observed in the HAPol sample (diffusion between sites after a mean residence time at each site), with correlation times on the picosecond time-scale, are similar to those interpreted from QENS studies as kink propagation in lipid chains (König and Sackmann 1996) and in 1,2-dimyristoyl-*sn*-glycero-3-phosphocholine (Trapp et al. 2010). The *gauche-trans-gauche* kink is the simplest higher-order defect of lipid chains. Its spontaneous generation and diffusion can be modeled as jump diffusion. These defects exist already in the gel phase. MD simulations show that their number increases monotonically with temperature, without any remarkable discontinuity at the phase transition (König and Sackman 1996). The QENS data on A8-35, consistent with jump diffusion, along with the latter's occurrence in both the gel and liquid crystal states of lipid chains, suggest that kink formation and propagation also exists in APol chains, probably independently of whether they are in the core of the A8-35 particle or in contact with membrane protein hydrophobic surfaces.

The other motions in A8-35 particles detected by QENS most likely correspond to local reorientational dynamics of the backbone CH and CH_2 and side-chain CH_2 and CH_3 groups. Such motions have been observed previously by QENS on purple membranes from *Halobacterium salinarum* at different hydration levels (Fitter et al. 1996, 1997).

Comparison with Lipids in Membranes

Lipids constitute the natural surroundings of MPs, in which they are stable and active, and it is of interest to compare the dynamics of such an environment with that of the A8-35 particle hydrophobic core. Neutron diffraction studies of glycolipids in purple membranes (Weik et al. 1998) and MD simulations on lipid interactions with aquaporins (Stansfeld et al. 2013) suggest that specific lipid/MP interactions occur mainly at the lipid head-group level and hydrophobic/hydrophilic interface, with softer transient interactions between the apolar protein surface and the lipid chains. Interestingly, lipid MSDs measured by neutron scattering in bilayers and around MPs in membranes (using deuterium labeling to distinguish protein and lipid motions) are very similar to one another (Frölich et al. 2009). This suggests that insertion of the MP does not greatly perturb the lipid environment, which acts as viscous medium around the protein.

It is useful to recall that a natural lipid environment will have a different fluidity depending on factors such as head-group hydration, chain composition, and temperature. In lipid membranes, water penetrates around the head-groups, increasing the area per head-group in the membrane plane. This entails a looser packing of the hydrocarbon chains and more flexibility. Early neutron diffraction experiments on purple membranes have shown that, at low hydration, the lipid component of the membrane occupies a smaller volume and 'presses' against BR (Rogan and Zaccai 1981; Zaccai 1987). Under similar conditions, BR is less active than at high hydration (Váró and Lanyi 1991). The hypothesis that the higher rigidity of the lipid environment inhibits MP functional dynamics is supported by neutron scattering, which shows significantly lower MSD for the dry purple membrane compared to the hydrated one (Ferrand et al. 1993).

It is to be expected that A8-35 particle core dynamics will also depend on steric constraints arising from the nature and distribution of grafted chains and from interactions of the hydrophilic groups in the outer shell between them and with the solvent. The radial density of solvation around the APol particle, represented by the distribution of Na^+ counterions and H_2O molecules, calculated from all-atom MD data (Perlmutter et al. 2011), is shown in Fig. 6 (bottom). The water density is $\sim$34 mol nm^{-3}, at a distance of 4 nm away from the center of the particle, as observed in the bulk for this water model at 303 K (Jorgensen and Jenson 1998; Klauda et al. 2006) and $\sim$15 mol nm^{-3} at the level of the carboxylate-rich particle surface. It is interesting to note, in this context, that MP/A8-35 complexes can be frozen (Gohon et al. 2008; Feinstein et al. 2014) or dried to $\sim$50 % relative humidity (Polovinkin et al. 2014) without denaturing the protein. This suggests that the general arrangement of the complexes is probably preserved under these conditions. In the partially dried state of BR/A8-35 complexes, however, resonance Raman spectra differ somewhat from those observed with hydrated purple membrane or with BR/A8-35 complexes kept in solution, in a way consistent with a

slowing down of the photocycle (longer life time of the M state; see Polovinkin et al. 2014). This is reminiscent of the functional effects observed upon drying native purple membrane (Váró and Lanyi 1991) and suggests that, upon partial dehydration, the APol belt surrounding BR also becomes more rigid. This hypothesis could be examined both experimentally and by MD simulations.

Effects of Amphipols on Membrane Protein Dynamics

With respect to how MP dynamics may be affected by an APol environment, the neutron scattering and MD data and the comparison with lipids favor a picture in which the hydrophobic transmembrane surface of the protein is surrounded by an environment similar to the core of the A8-35 particle, of comparable local fluidity to that of the hydrophobic region of a lipid bilayer, whereas the relatively stiff backbone of the polymer provides the interface with the solvent. This picture is in qualitative agreement with MD simulations of A8-35 interactions with the MP OmpX (Perlmutter et al. 2014). As with lipid head-groups and chains, shell and core dynamics in A8-35 are not uncorrelated: A8-35 particle core dynamics, and, by extension, that of the APol belt surrounding MPs, will also depend on steric considerations based on the nature and distribution of grafted chains and on interactions of the hydrophilic groups in the shell with both the solvent and the MP.

As mentioned in the introduction, biochemical observations have led to the hypothesis that APols may damp large-scale conformational excursions by the transmembrane domains of MPs. This phenomenon, the "Gulliver effect", has been postulated to result from the activation free energy penalty for rearranging the backbone of the polymer to adapt to transconformations of the protein's transmembrane surface (Picard et al. 2006; Popot et al. 2003, 2011; Zoonens and Popot 2014). It provides a tentative explanation for the correlation observed between stabilization of the sarcoplasmic calcium ATPase and inhibition of its enzymatic cycle (Picard et al. 2006). Its existence is supported by the observation that stabilization of OmpA by A8-35 against urea-induced denaturation is not thermodynamic in its origin, but kinetic: the free energy barrier for moving from the folded to the unfolded state is strongly increased, resulting in a much slower denaturation rate (Pocanschi et al. 2013; Kleinschmidt and Popot 2014). Such a view tallies with the MD comparison of the dynamics of OmpX in complex with either A8-35, a detergent, or a lipid bilayer, which shows that the APol-trapped protein undergoes conformational excursions of restricted amplitude as compared to the detergent-solubilized one and even that spanning a bilayer (Perlmutter et al. 2014). The present neutron scattering measurements are consistent with the view that damping of MP dynamics, as compared to that in lipids, is more likely to originate from the dynamics of the polymer's backbone rather than from that of the octyl chains.

Acknowledgments Particular thanks are due to Michael Marek Koza and Bernhard Frick, ILL local contacts on IN6 and IN16, respectively. This work was supported by the French Centre National de la Recherche Scientifique (CNRS), by Université Paris–7 Denis Diderot, and by Grant "DYNAMO", ANR-11-LABX-0011-01 from the French "Initiative d'Excellence" Program. 'Computational resources were provided by the Minnesota Supercomputing Institute (MSI).

References

Althoff T, Mills DJ, Popot J-L, Kühlbrandt W (2011) Assembly of electron transport chain components in bovine mitochondrial supercomplex $I_1III_2IV_1$. EMBO J 30:4652–4664

Bée M (1988) Quasielastic neutron scattering: principles and applications in solid state chemistry. Biology and Materials Science Adam Hilger, Philadelphia

Bowie JU (2001) Stabilizing membrane proteins. Curr Opin Struct Biol 11:397–402

Champeil P, Menguy T, Tribet C, Popot J-L, le Maire M (2000) Interaction of amphipols with the sarcoplasmic reticulum Ca^{2+}-ATPase. J Biol Chem 275:18623–18637

Charvolin D, Picard M, Huang L-S, Berry EA, Popot J-L (2014) Solution behavior and crystallization of cytochrome bc_1 in the presence of amphipols. J Membr Biol. doi:10.1007/s00232-014-9694-4

Etzkorn M, Zoonens M, Catoire LJ, Popot J-L, Hiller S (2014) How amphipols embed membrane proteins: global solvent accessibility and interaction with a flexible protein terminus. J Membr Biol. doi:10.1007/s00232-014-9657-9

Feinstein HE, Tifrea D, Sun G, Popot J-L, de la Maza LM, Cocco MJ (2014) Long-term stability of a vaccine formulated with the amphipol-trapped major outer membrane protein from *Chlamydia trachomatis*. J Membr Biol. doi:10.1007/s00232-014-9693-5

Ferrand M, Dianoux AJ, Petry W, Zaccai G (1993) Thermal motions and function of bacte-rio-rhod-opsin in purple membranes: effects of temperature and hydration studied by neutron scattering. Proc Natl Acad Sci USA 90:9668–9672

Fitter J, Lechner RE, Büldt G, Dencher NA (1996) Internal molecular motions of bacteriorhodopsin: hydration-induced flexibility studied by quasielastic incoherent neutron scattering using oriented purple membranes. Proc Natl Acad Sci USA 193:7600–7605

Fitter J, Lechner RE, Dencher NA (1997) Picosecond molecular motions in bacteriorhodopsin from neutron scattering. Biophys J 73:2126–2137

Frölich A, Gabel F, Jasnin M, Lehnert U, Oesterhelt D, Stadler AM, Tehei M, Weik M, Wood K, Zaccai G (2009) From shell to cell: neutron scattering studies of biological water dynamics and coupling to activity. Faraday Discuss 41:117–130 discussion 175-207

Garavito RM, Ferguson-Miller S (2001) Detergents as tools in membrane biochemistry. J Biol Chem 276:32403–32406

Giusti F, Popot J-L, Tribet C (2012) Well-defined critical association concentration and rapid adsorption at the air/water interface of a short amphiphilic polymer, amphipol A8-35: a study by Förster resonance energy transfer and dynamic surface tension measurements. Langmuir 28:10372–10380

Giusti F, Rieger J, Catoire L, Qian S, Calabrese AN, Watkinson TG, Casiraghi M, Radford SE, Ashcroft AE, Popot J-L (2014)

Synthesis, characterization and applications of a per-deuterated amphipol. J Membr Biol. doi:10.1007/s00232-014-9656-x
Gohon Y, Popot J-L (2003) Membrane protein-surfactant complexes. Curr Opin Colloid Interface Sci 8:15–22
Gohon Y, Pavlov G, Timmins P, Tribet C, Popot J-L, Ebel C (2004) Partial specific volume and solvent interactions of amphipol A8-35. Anal Biochem 334:318–334
Gohon Y, Giusti F, Prata C, Charvolin D, Timmins P, Ebel C, Tribet C, Popot J-L (2006) Well-defined nanoparticles formed by hydrophobic assembly of a short and polydisperse random terpolymer, amphipol A8-35. Langmuir 22:1281–1290
Gohon Y, Dahmane T, Ruigrok R, Schuck P, Charvolin D, Rappaport F, Timmins P, Engelman DM, Tribet C, Popot J-L, Ebel C (2008) Bacteriorhodopsin/amphipol complexes: structural and functional properties. Biophys J. 94:3523–3537
Huynh KW, Cohen MR, Moiseenkova-Bell VY (2014) Application of amphipols for structu-re-functional analysis of TRP channels. J Membr Biol. doi:10.1007/s00232-014-9684-6
Jasnin M, van Eijck L, Koza MM, Peters J, Laguri C, Lortat-Jacob H, Zaccai G (2010) Dynamics of heparan sulfate explored by neutron scattering. Phys Chem Chem Phys 12:3360–3362
Jorgensen WL, Jenson C (1998) Temperature dependence of TIP3P, SPC, and TIP4P water from NPT Monte Carlo simulations: seeking a temperature of maximum density. J Comp Chem 19:1179–1186
Klauda JB, Kucerka N, Brooks BR, Pastor RW, Nagle JF (2006) Simulation-based methods for interpreting X-ray data from lipid bilayers. Biophys J 90:2796–2807
Kleinschmidt JH, Popot J-L (2014) Folding and stability of integral membrane proteins in amphipols. Arch Biochem Biophys (in press)
König S, Sackmann E (1996) Molecular and collective dynamics of lipid bilayers. Curr Opin Colloid Interface Sci 1:78–82
Liao M, Cao E, Julius D, Cheng Y (2013) Structure of the TRPV1 ion channel determined by electron cryo-microscopy. Nature 504:107–112
Liao M, Cao E, Julius D, Cheng Y (2014) Single particle electron cryo-microscopy of a mammalian ion channel. Curr Opin Struct Biol 27:1–7
MacKerell AD Jr, Bashford D, Bellott M, Dunbrack RL Jr, Evanseck JD, Field MJ, Fischer S, Gao J, Guo H, Ha S, Joseph-McCarthy D, Kuchnir L, Kuczera K, Lau FTK, Mattos C, Michnick S, Ngo T, Nguyen DT, Prodhom B, Reiher WR III, Roux B, Schlenkrich M, Smith JC, Stote R, Straub J, Watanabe M, Wiórkiewicz-Kuczera J, Yin D, Karplus M (1998) All-atom empirical potential for molecular modeling and dynamics studies of proteins. J Phys Chem B 102:3586–3616
Marrink SJ, Risselada HJ, Yefimov S, Tieleman DP, de Vries AH (2007) The MARTINI force field: coarse grained model for biomolecular simulations. J Phys Chem B 111:7812–7824
Natali F, Castellano C, Pozzi D, Congiu-Castellano A (2005) Dynamic properties of an orient-ed lipid/DNA complex studied by neutron scattering. Biophys J 88:1081–1090
Perez J, Zanotti JM, Durand D (1999) Evolution of the internal dynamics of two globular proteins from dry powder to solution. Biophys J 77:454–469
Perlmutter JD, Drasler WJ, Xie W, Gao J, Popot J-L, Sachs JN (2011) All-atom and coarse-grained molecular dynamics simulations of a membrane protein stabilizing polymer. Langmuir 27:10523–10537
Perlmutter JD, Popot J-L, Sachs JN (2014) Molecular dynamics simulations of a membrane protein/amphipol complex. J Membr Biol. doi:10.1007/s00232-014-9690-8
Picard M, Dahmane T, Garrigos M, Gauron C, Giusti F, le Maire M, Popot J-L, Champeil P (2006) Protective and inhibitory effects of various types of amphipols on the Ca^{2+}-ATPase from sarcoplasmic reticulum: a comparative study. Biochemistry 45:1861–1869
Planchard N, Point E, Dahmane T, Giusti F, Renault M, Le Bon C, Durand G, Milon A, Guittet E, Zoonens M, Popot J-L, Catoire LJ (2014) The use of amphipols for solution NMR studies of membrane proteins: advantages and limitations as compared to other solubilizing media. J Membr Biol. doi:10.1007/s00232-014-9654-z
Pocanschi C, Popot J-L, Kleinschmidt JH (2013) Folding and stability of outer membrane protein A (OmpA) from *Escherichia coli* in an amphipathic polymer, amphipol A8-35. Eur Biophys J 42:103–118
Polovinkin V, Balandin T, Volkov O, Round E, Borshchevskiy V, Utrobin P, von Stetten D, Royant A, Willbold D, Arzumanyan A, Popot J-L, Gordeliy V (2014) Nanoparticle surface enhanced Raman scattering of bacteriorhodopsin stabilized by amphipol A8-35. J Membr Biol. doi:10.1007/s00232-014-9701-9
Popot JL (2010) Amphipols, nanodiscs, and fluorinated surfactants: three non-conventional approaches to studying membrane proteins in aqueous solutions. Annu Rev Biochem 79:737–775
Popot J-L, Berry EA, Charvolin D, Creuzenet C, Ebel C, Engelman DM, Flötenmeyer M, Giusti F, Gohon Y, Hervé P, Hong Q, Lakey JH, Leonard K, Shuman HA, Timmins P, Warschawski DE, Zito F, Zoonens M, Pucci B, Tribet C (2003) Amphipols: polymeric surfactants for membrane biology research. Cell Mol Life Sci 60:1559–1574
Popot J-L, Althoff T, Bagnard D, Banères J-L, Bazzacco P, Billon-Denis E, Catoire LJ, Champeil P, Charvolin D, Cocco MJ, Crémel G, Dahmane T, de la Maza LM, Ebel C, Gabel F, Giusti F, Gohon Y, Goormaghtigh E, Guittet E, Kleinschmidt JH, Kühlbrandt W, Le Bon C, Martinez KL, Picard M, Pucci B, Rappaport F, Sachs JN, Tribet C, van Heijenoort C, Wien F, Zito F, Zoonens M (2011) Amphipols from A to Z. Annu Rev Biophys 40:379–408
Rogan PK, Zaccai G (1981) Hydration of purple membrane as a function of relative humidity. J Mol Biol 145:281–284
Rosenbusch JP (2001) Stability of membrane proteins: relevance for the selection of appropriate methods for high-resolution structure determinations. J Struct Biol 136:144–157
Stansfeld PJ, Jeffreys EE, Sansom MSP (2013) Multiscale simulations reveal conserved patterns of lipid interactions with aquaporins. Structure 21:810–819
Tehei M, Zaccai G (2005) Adaptation to extreme environments: macromolecular dynamics in complex systems. Biochim Biophys Acta 1724:404–410
Tehei M, Madern D, Pfister C, Zaccai G (2001) Fast dynamics of halophilic malate dehydrogenase and BSA measured by neutron scattering under various solvent conditions influencing protein stability. Proc Natl Acad Sci USA 98:14356–14361
Tehei M, Madern D, Franzetti B, Zaccai G (2005) Neutron scattering reveals the dynamic basis of protein adaptation to extreme temperature. J Biol Chem 280:40974–40979
Trapp M, Gutberlet T, Juranyi F, Unruh T, Demé B, Tehei M, Peters J (2010) Hydration dependent studies of highly aligned multilayer lipid membranes by neutron scattering. J Chem Phys 133:164505
Tribet C, Audebert R, Popot J-L (1996) Amphipols: polymers that keep membrane proteins soluble in aqueous solutions. Proc Natl Acad Sci USA 93:15047–15050
Váró G, Lanyi JK (1991) Distortions in the photocycle of bacteriorhodopsin at moderate dehydration. Biophys J 59:313–322
Venkatesan M, Hirtzel CS, Rajagopalan R (1985) The effect of colloidal forces on the self-diffusion coefficients in strongly interacting dispersions. J Chem Phys 82:5685–5695
Weik M, Patzelt H, Zaccai G, Oesterhelt D (1998) Localization of glycolipids in membranes by in vivo labeling and neutron diffraction. Mol Cell 1:411–419
Zaccai G (1987) Structure and hydration of purple membranes in different conditions. J Mol Biol 194:569–572

Zaccai G (2011) Neutron scattering perspectives for protein dynamics. J Non-Cryst Solids 357:615–621

Zaccai G (2013) The ecology of protein dynamics. Curr Phys Chem 3:9–16

Zoonens M, Popot J-L (2014) Amphipols for each season. J Membr Biol. doi:10.1007/s00232-014-9666-8

Zoonens M, Catoire LJ, Giusti F, Popot J-L (2005) NMR study of a membrane protein in detergent-free aqueous solution. Proc Natl Acad Sci USA 102:8893–8898